the assumption that we can model such interactions by neglecting the atom-atom terms for the O---C pair is not well understood, although it appears to describe the CO_2-H_2O dimer quite well. Further theoretical work on modelling such interactions is clearly required.

Discussion and Conclusion

We have attempted to paint a picture (albeit with a very broad brush) of the sort of results that can be obtained by computing intermolecular energies from the experimental electron density distributions in molecular crystals. There are many details that deserve further consideration. However, we believe that we have achieved our principal goal. This was to demonstrate that the multipole expansion of $\rho(r)$ about the atomic nuclei, as obtained directly from diffraction data, contains valuable information about the energetics and configurations of molecular systems, particularly those that are hydrogen bonded. The advent of such a direct approach for estimating E_{es} may become useful in assessing the importance of various types of hydrogen bonding in crystals. In the past, such judgements have tended to rely heavily on various geometrical criteria involving interatomic distances and angles, such as those proposed by Hamilton and Ibers[63] and others subsequently.

However, we must be cautious in the interpretation of our results, for several reasons. First, and most obviously, the energies we have computed have associated with them quite large esds. This point has not been addressed in previous studies,[2,3,9] but it deserves consideration in the future. Values of E_{es} are proportional to products of pairs of experimentally determined $C_{lm\pm}$ parameters. Hence the relative error in a property such as E_{es} should be about double when compared with a property such as the charge density which is linearly dependent on $C_{lm}^{\pm}$. From our calculations for the crystal complex of thiourea and parabanic acid, it seems unlikely that significant values of E_{es} can be obtained from X-ray diffraction data collected at room temperature. In order to draw definitive conclusions about molecular interaction energies from diffraction data alone, high-resolution Bragg intensity data are needed at or beyond the levels of precision which are presently attainable.

Secondly, we note that the simple model used to approximate the remaining components of the interaction energy (repulsion, dispersion, polarization, charge-transfer, etc.) is far from fully optimized. The main reason it appears to work so well at present is because deficiencies are hidden by the large values of $\sigma(E_{es})$. However, we must seek a better understanding of the approximation used to describe the hydrogen bond, and in particular its extension to C=O---C type interactions, as discussed in this work.

Acknowledgment. This work was supported by Grant HL-20350 from the National Institutes of Health. We are grateful to Joan Klinger for technical assistance.

Registry No. Imidazole, 288-32-4; 9-methyladenine, 700-00-5; cytosine monohydrate, 6020-40-2; urea, 57-13-6; parabonic acid-thiourea (1:1), 58343-74-1; alloxan, 50-71-5.

(63) Hamilton, W. C.; Ibers, J. A. *Hydrogen Bonding in Solids*; Benjamin: New York, 1968.

Magnetic Ordering of $Mn^{II}Cu^{II}$ Bimetallic Chains: Design of a Molecular-Based Ferromagnet

Olivier Kahn,*† Yu Pei,† Michel Verdaguer,† Jean Pierre Renard,‡ and Jorunn Sletten§

Laboratoire de Spectrochimie des Elêments de Transition, U.A. No. 420, Universitê de Paris Sud, 91405 Orsay, France, Institut d'Electronique Fondamentale, U.A. No. 022, Universitê de Paris Sud, 91405 Orsay, France, and Department of Chemistry, University of Bergen, 5007 Bergen, Norway. *Received March 26, 1987*

Abstract: The compound $MnCu(pbaOH)(H_2O)_3$ (**2**) with pbaOH = 2-hydroxy-1,3-propylenebis(oxamato) has been synthesized, and its crystal structure has been solved. It crystallizes in the orthorhombic system, space group $P2_12_12_1$, with a = 12.351 (7) Å, b = 21.156 (11) Å, c = 5.073 (10) Å, and Z = 4 (MnCu units). The structure consists of ordered bimetallic chains running along the b axis with Mn^{II} and Cu^{II} ions bridged by oxamato groups. The shortest interchain metal-metal separations are Mn···Cu = 5.751 Å in the a direction and Mn···Mn = Cu···Cu = 5.073 Å in the c direction. The magnetic properties of **2** have been investigated and compared to those of $MnCu(pba)(H_2O)_3 \cdot 2H_2O$ (**1**) with pba = 1,3-propylenebis(oxamato), which has been previously described. **1** has the same chain structure as **2**, but along the a direction the shortest separations are of the type Mn···Mn and Cu···Cu instead of Mn···Cu. In the $30 < T < 300$ K temperature range, the $\chi_M T$ versus T plots for **1** and **2** are identical and characteristic of antiferromagnetically coupled ordered bimetallic chains with a minimum of $\chi_M T$ at 115 K. Upon cooling below 30 K, $\chi_M T$ increases much faster for **2** than for **1** and diverges around 5 K. **1** orders antiferromagnetically at 2.2 K with a small canting along the a direction. In contrast, **2** orders ferromagnetically at 4.6 K. The temperature dependences of the magnetization M for **2** along the three directions of the lattice have been investigated and have shown that the c axis is the easy magnetization axis. The M versus the field H plot has also been studied for a polycrystalline sample at various temperatures between 4.2 and 1.3 K. A hysteresis loop characteristic of a soft magnet has been obtained. At 1.3 K, the remnant magnetization is 2.25×10^3 cm^3 mol^{-1} G and the coercive field around 50 G. The mechanism of the 3D magnetic ordering in **1** and **2** has been discussed. The key role has been suggested to be the relative positions of the chains along the a direction.

For a few years, we have participated in the efforts to design molecular systems ordering ferromagnetically. Molecular in this context means that we use the synthesis methods of the molecular chemistry—we work in solution, with mild conditions of temperature and pressure—and that we attempt to build the three-dimensional lattice by assembling molecular bricks in a controllable fashion. One possible approach along this line consists of synthesizing molecular entities with a large spin multiplicity in their ground state and then of assembling them within the crystal lattice in a ferromagnetic fashion.[1-3] A slightly different approach

† Laboratoire de Spectrochimie des Elêments de Transition, Universitê de Paris Sud.
‡ Institut d'Electronique Fondamentale, Universitê de Paris Sud.
§ University of Bergen.

(1) Iwamura, H.; Sugawara, T.; Itoh, K.; Takui, T. *Mol. Cryst. Liq. Cryst.* **1985**, *125*, 251.

0002-7863/88/1510-0782$01.50/0

consists of assembling the molecular bricks in such a way as to obtain a low-dimensional system with a nonzero resulting spin in the ground state and then coupling the chains or the layers again in a ferromagnetic fashion.[4] In both approaches, the first step requires the design of a system with a highly magnetic ground state. This may be achieved by coupling the nearest-neighbor magnetic centers in a ferromagnetic way.[5] Several strategies have been proposed so far to obtain such a ferromagnetic interaction,[1-3,6-11] and some examples of design of ferromagnetically coupled molecules have been reported.[5,12-14] One-dimensional systems with ferromagnetic intrachain interactions have also been described.[15,16] However, all these strategies favoring the parallel alignment of local spins are based on symmetry conditions that are often difficult to realize. An alternative solution consists of using heteropolymetallic systems.[17] Even if the interaction between nearest neighbors is antiferromagnetic, as it is most frequently, the ground state can be magnetic owing to the noncompensation of the local spins. In some cases, not only the ground state is magnetic but in addition its spin multiplicity is higher than those of the first excited states, so that a ferromagnetic-like behavior may be obtained in the low-temperature range.[18] "Ferromagnetic-like behavior" means here that the product of the molar magnetic susceptibility times the temperature $\chi_M T$ increases upon cooling down, as occurs for a genuine ferromagnetically coupled system. Such a situation can happen when the spin-state structure is irregular, i.e. when the spin multiplicity of the molecular states does not vary monotonically versus the energy of these states. In a recent paper, we pointed out that a $Mn^{II}Cu^{II}Mn^{II}$ trinuclear species provided a spectacular example of a system exhibiting a ferromagnetic-like behavior owing to the irregularity of the spin-state structure.[18]

The concept of irregular spin-state structure is not limited to trinuclear species or other polynuclear molecular entities but can be extended to the ordered bimetallic chains, of which several examples have recently been reported.[19-22] Let us consider a $Mn^{II}Cu^{II}$ chain of this kind with an antiferromagnetic interaction between the adjacent $S_{Mn} = {}^5/_2$ and $S_{Cu} = {}^1/_2$ local spins. The ground state may be schematized as

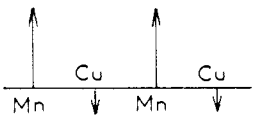

and in absence of any interaction, a 1D magnetic ordering is expected at 0 K, with a divergence of the product $\chi_M T$, χ_M being here the molar magnetic susceptibility per MnCu unit. This behavior may be defined as the one-dimensional ferrimagnetism. In fact, when the molecular entities with a magnetic ground state or the ferrimagnetic chains are assembled within the crystal lattice, intermolecular or interchain interactions are created. Even if these interactions are very weak as compared to the intramolecular or intrachain interactions, they lead to the onset of a magnetic order at a nonzero temperature. This order may be antiferromagnetic or ferromagnetic; most often it is antiferromagnetic. The problem at hand is to succeed in favoring the ferromagnetic ordering. It is clear that this is not all a trivial problem. We already noticed how problematic achieving an intramolecular or intrachain ferromagnetic interaction was. Achieving an intermolecular or interchain ferromagnetic interaction is obviously even more problematic. The factors governing the crystal packing are extremely subtle and hard to control. If the molecular engineering is a difficult art, the crystal engineering is a challenge.

The goal of this paper is to approach the problem of the crystal engineering of the molecular ferromagnets. For that, we shall compare two compounds, chemically very similar, of formula $MnCu(pba)(H_2O)_3 \cdot 2H_2O$ (**1**) and $MnCu(pbaOH)(H_2O)_3$ (**2**) (pba = 1,3-propylenebis(oxamato); pbaOH = 2-hydroxy-1,3-propylenebis(oxamato)). Both are obtained by polymerization of a copper(II) mononuclear dianion, $[Cu(pba)]^{2-}$ or $[Cu(pbaOH)]^{2-}$, represented here as

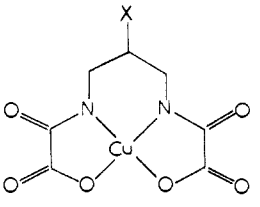

$[Cu(pba)]^{2-}$, X = H
$[Cu(pbaOH)]^{2-}$, X = OH

with Mn^{II}. **1** and **2**, as expected, have very similar chain structures, but the relative positions of the chains within the lattice are slightly different, leading to completely different magnetic properties in the low-temperature range. **1** orders antiferromagnetically and **2** ferromagnetically. **2** may be considered as one of the very few genuine molecular ferromagnets. We shall successively study the crystal structure of the compounds, their magnetic susceptibility, and their magnetization. Finally, we shall try to rationalize these properties and understand the mechanism of the magnetic ordering. A preliminary communication of this work has already been published.[22]

Experimental Section

Synthesis of 2. It was carried out in three steps. The first one concerns the synthesis of the 2-hydroxy-1,3-propylenebis(oxamide) (**3**); 10 mL of an ethanol solution containing 5 mmol of 2-hydroxy-1,3-propylenediamine was added to 50 mL of an ethanol solution containing 10 mmol of ethyl oxamate. The mixture was heated at reflux for 1 h. **3** precipitated as a white polycrystalline powder. The second step consists of synthesizing the mononuclear complex $Na_2[Cu(pbaOH)] \cdot 3H_2O$ (**4**) from 5 mmol of **3** and 20 mmol of NaOH in 50 mL of water, heated at 60 °C for a few minutes. An aqueous solution containing 5 mmol of $Cu(NO_3)_2 \cdot 3H_2O$ (10 mL) was then added, and the mixture was heated at reflux until complete hydrolysis of the primary amide groups (about 3 h). The solution was filtered and reduced to 20 mL and **4** was precipitated upon addition of ethanol. Finally, a light blue single crystal of **2** was obtained by slow diffusion of 50 mL of aqueous solutions containing 0.5 mmol of $Na_2[Cu(pbaOH)] \cdot 3H_2O$ and $Mn(ClO_4)_2 \cdot 6H_2O$, respectively, in an H-shaped tube within about 3 months. Anal. Calcd for $C_7H_{12}N_2O_{10}CuMn$ (**2**): C, 20.88; H, 3.00; N, 6.96; Cu, 15.78; Mn, 13.64. Found: C, 20.95; H, 3.18; N, 6.97; Cu, 16.01; Mn, 13.79. The stretching vibration of the OH group appears at 3570 cm^{-1}. The syn-

(2) Sagawura, T.; Bandow, S.; Kimura, K.; Iwamura, H.; Itoh, K. *J. Am. Chem. Soc.* **1986**, *108*, 368.
(3) Teki, Y.; Takui, T.; Itoh, K.; Iwamura, H.; Kobayashi, K. *J. Am. Chem. Soc.* **1986**, *108*, 2147.
(4) Miller, J.; Calabrese, J. C.; Rommelmann, H.; Chittipeddi, S. R.; Zhang, J. H.; Reiff, W. M.; Epstein, A. J. *J. Am. Chem. Soc.* **1987**, *109*, 769.
(5) Cairns, C. J.; Busch, D. H. *Coord. Chem. Rev.* **1986**, *69*, 1 and references therein.
(6) Kahn, O. *Angew. Chem., Int. Ed. Engl.* **1985**, *24*, 834 and references therein.
(7) Charlot, M. F.; Kahn, O.; Chaillet, M.; Larrieu, C. *J. Am. Chem. Soc.* **1986**, *108*, 2574.
(8) McConnell, H. M. *Proc. Robert A. Welch Found. Conf. Chem. Res.* **1967**, *11*, 144.
(9) Breslow, R. *Pure Appl. Chem.* **1982**, *54*, 927.
(10) Breslow, R. *Mol. Cryst. Liq. Cryst.* **1985**, *125*, 261.
(11) Torrance, J. B.; Oostra, S.; Nazzal, A. *Synth. Metals*, in press.
(12) Kahn, O.; Galy, J.; Journaux, Y.; Jaud, J.; Morgenstern-Badarau, I. *J. Am. Chem. Soc.* **1982**, *104*, 2165.
(13) Journaux, Y.; Kahn, O.; Zarembowitch, J.; Galy, J. *J. Am. Chem. Soc.* **1983**, *105*, 7585.
(14) Kahn, O.; Prins, R.; Reedijk, J.; Thompson, J. S. *Inorg. Chem.* **1987**, *26*, 3557.
(15) Willett, R. D.; Gaura, R. M.; Landee, C. P. In *Extended Linear Chain Compounds*; Miller, J. S., Ed.; Plenum: New York, London, 1983; Vol. 3, p 143.
(16) Hatfield, W. E.; Estes, W. E.; Marsch, W. E.; Pickens, M. W.; Ten Haar, L. W.; Weller, R. R. In *Extended Linear Chain Compounds*; Miller, J. S., Ed.; Plenum: New York, London, **1983**, Vol. 3, p 43.
(17) Kahn, O. *Struct. Bonding (Berlin)* **1987**, *68*, 89.
(18) Pei, Y.; Journaux, Y.; Kahn, O. *Inorg. Chem.*, in press.
(19) Gleizes, A.; Verdaguer, M. *J. Am. Chem. Soc.* **1981**, *103*, 7373; **1984**, *106*, 3727.
(20) Beltran, D.; Escriva, E.; Drillon, M. *J. Chem. Soc., Faraday Trans. 2* **1982**, *78*, 1773.
(21) Drillon, M.; Coronado, E.; Beltran, D.; Georges, R. *Chem. Phys.* **1983**, *79*, 449.
(22) Pei, Y.; Verdaguer, M.; Kahn, O.; Sletten, J.; Renard, J. P. *J. Am. Chem. Soc.* **1986**, *108*, 7428; *Inorg. Chem.* **1987**, *26*, 138.

Table I. Information Concerning the Crystallographic Data Collection and Refinement Conditions for $MnCu(pbaOH)(H_2O)_3$ (**2**)

mol formula	$CuMnC_7H_{12}N_2O_{10}$
formula wt	402.66
space gp	$P2_12_12_1$
temp at cryst, K	294
unit cell	
a, Å	12.351 (7)
b, Å	21.156 (11)
c, Å	5.073 (10)
V, Å^3	1326 (4)
Z	4
D_x, g cm^{-3}	2.018
μ(Mo Kα), cm^{-1}	25.76
cryst size, mm	0.23 × 0.06 × 0.51
instrument	CAD-4
scan type	ω
scan range, $\Delta\omega$, deg	2.8 + 0.35 tan θ
scan speed, deg/min	6.7–1.25
radiation (λ, Å)	monochromated Mo Kα (0.71073)
max 2θ, deg	45
no. reflcns measd	1054
no. obsd reflcns, NO	960
limit of obsd reflcns	$F_o > 2\sigma$
no. variables refined, NV	85
agreement factors:[a]	
R	0.056
R_w	0.058
s	2.55

[a] Agreement factors are defined as follows: $R = \sum||F_o| - |F_c||/\sum|F_o|$; $R_w = [\sum w(|F_o| - |F_c|)^2/[w|F_o|^2]]^{1/2}$; $s = [\sum w(|F_o| - |F_c|)^2/(NO - NV)]^{1/2}$. The weighting scheme is defined by $w = 1/\sigma_F^2$; $\sigma_F = \sigma_I/(ILp)^{1/2}$; and $\sigma_I = [\sigma_c^2 + (0.02N_{net})^2]^{1/2}$. Atomic scattering factors and programs used are those of ref 37 and 38.

Table II. Atomic Parameters for $MnCu(pbaOH)(H_2O)_3$ (**2**)[a]

atom	x	y	z	B_{eq} or B, Å^2
Cu	0.5510 (1)	0.16877 (6)	0.4152 (3)	1.75 (3)
Mn	0.5310 (1)	−0.08258 (8)	0.2625 (4)	1.78 (4)
O1	0.4655 (6)	−0.0103 (4)	0.520 (2)	1.8 (2)*
O2	0.6232 (6)	−0.0000 (4)	0.149 (2)	2.0 (2)*
O3	0.6344 (6)	0.1035 (4)	0.225 (2)	2.1 (2)*
O4	0.5996 (6)	0.2366 (3)	0.170 (2)	1.4 (2)*
O5	0.4137 (6)	0.3390 (4)	0.483 (2)	1.6 (2)*
O6	0.5618 (6)	0.3379 (3)	0.084 (2)	1.4 (1)*
O7	0.2613 (7)	0.1587 (4)	0.456 (2)	2.6 (2)*
O8	0.6576 (7)	−0.1132 (4)	0.545 (2)	2.6 (2)*
O9	0.4003 (7)	−0.0645 (4)	−0.022 (2)	3.1 (2)*
O10	0.6960 (7)	0.2084 (4)	0.689 (2)	2.8 (2)*
N1	0.4719 (7)	0.0987 (4)	0.561 (2)	1.7 (2)*
N2	0.4548 (8)	0.2335 (4)	0.549 (2)	1.5 (2)*
C1	0.5922 (9)	0.0478 (5)	0.266 (3)	1.7 (2)*
C2	0.5041 (9)	0.0442 (6)	0.469 (3)	1.7 (2)*
C3	0.382 (1)	0.1015 (6)	0.746 (3)	2.4 (3)*
C4	0.3137 (9)	0.1605 (5)	0.719 (3)	1.6 (2)*
C5	0.3731 (9)	0.2225 (5)	0.755 (3)	1.5 (2)*
C6	0.4670 (8)	0.2869 (5)	0.435 (2)	0.8 (2)*
C7	0.5484 (9)	0.2885 (5)	0.212 (2)	1.5 (2)*

[a] Starred values refer to atoms refined isotropically. Anisotropically refined atoms are given in the form of the isotropic equivalent thermal parameter $B_{eq} = {}^4/_3\sum_i\sum_j\beta_{ij}a_ia_j$.

thesis of **1** has been previously described.[22]

Crystallographic Data Collection and Structure Determination. Information concerning conditions for crystallographic data collection and structure refinement is summarized in Table I. The only crystal available for X-ray investigation had a wide mosaic spread and split reflections. This causes comparatively low accuracy in the determined cell dimensions as well as in the intensity measurements. The three reference reflections monitored during data collection showed no significant deterioration. Absorption correlation was not performed, as other errors in the data were judged to be far more serious.

The structure was solved by direct methods. The metal ions and most of the bridging group could be distinguished in the E map; the remaining non-hydrogen atoms were located in a subsequent difference Fourier map. Anisotropic refinement of all atoms was attempted, but as the temperature factor of C6 was not positive-definite, only Cu and Mn were anisotropically refined in the final cycles. Hydrogen atoms attached to atoms O7, O9, and O10 were located in a difference map; those attached to O8 could not be unambiguously located. Idealized positions for hydrogen atoms attached to C3, C4, and C5 were calculated. The hydrogen atoms were included in the final structure factor calculations, but the data did not warrant their refinement. The refinement converged at $R = 0.056$, $R_w = 0.058$, and $S = 2.55$. Final atomic parameters for non-hydrogen atoms are listed in Table II. Anisotropic thermal parameters for Cu and Mn are given in Table VI and the hydrogen positional parameters in Table VII (supplementary material).

Table III. Bond Distances Involving Non-Hydrogen Atoms in $MnCu(pbaOH)(H_2O)_3$ (**2**)[a]

atoms	dist, Å	atoms	dist, Å
Cu–O3	1.974 (5)	O3–C1	1.305 (8)
Cu–O4	1.991 (5)	O4–C7	1.285 (8)
Cu–O10	2.417 (6)	O5–C6	1.307 (8)
Cu–N1	1.923 (6)	O6–C7	1.243 (8)
Cu–N2	1.936 (6)	O7–C4	1.486 (10)
Mn–O1	2.169 (5)	N1–C2	1.306 (9)
Mn–O2	2.162 (5)	N1–C3	1.456 (11)
Mn–O5[a]	2.185 (5)	N2–C5	1.472 (10)
Mn–O6[a]	2.179 (5)	N2–C6	1.278 (8)
Mn–O8	2.216 (6)	C1–C2	1.499 (11)
Mn–O9	2.199 (6)	C3–C4	1.513 (10)
O1–C2	1.274 (8)	C4–C5	1.514 (10)
O2–C1	1.233 (9)	C6–C7	1.511 (10)

[a] Symmetry operation: (a) $1 - x, y - {}^1/_2, {}^1/_2 - z$.

Table IV. Bond Angles Involving Non-Hydrogen Atoms in $MnCu(pbaOH)(H_2O)_3$ (**2**)

atoms[a]	angle, deg	atoms[a]	angle, deg
O3–Cu–O4	92.4 (2)	Cu–O3–C1	110.3 (5)
O3–Cu–O10	97.9 (2)	Cu–O4–C7	111.3 (5)
O3–Cu–N1	85.0 (2)	Mn[b]–O5–C6	112.1 (4)
O3–Cu–N2	170.4 (3)	Mn[b]–O6–C7	113.1 (5)
O4–Cu–O10	83.5 (2)	Cu–N1–C2	112.9 (5)
O4–Cu–N1	161.5 (2)	Cu–N1–C3	127.2 (5)
O4–Cu–N2	83.9 (2)	C2–N1–C3	119.9 (6)
O10–Cu–N1	115.0 (2)	Cu–N2–C5	123.9 (4)
O10–Cu–N2	90.5 (2)	Cu–N2–C6	113.2 (5)
N1–Cu–N2	95.7 (2)	C5–N2–C6	122.9 (6)
O1–Mn–O2	77.7 (2)	O2–C1–O3	122.7 (7)
O1–Mn–O5[a]	175.0 (2)	O2–C1–C2	121.0 (7)
O1–Mn–O6[a]	97.6 (2)	O3–C1–C2	116.4 (7)
O1–Mn–O8	94.6 (2)	O1–C2–N1	127.7 (7)
O1–Mn–O9	89.9 (2)	O1–C2–C1	117.2 (7)
O2–Mn–O5[a]	107.3 (2)	N1–C2–C1	115.0 (7)
O2–Mn–O6[a]	174.4 (2)	N1–C3–C4	113.6 (7)
O2–Mn–O8	92.1 (2)	O7–C4–C3	107.6 (7)
O2–Mn–O9	94.1 (2)	O7–C4–C5	109.9 (6)
O5[a]–Mn–O6[a]	77.4 (6)	C3–C4–C5	115.8 (6)
O5[a]–Mn–O8	85.8 (2)	N2–C5–C4	112.6 (7)
O5[a]–Mn–O9	89.3 (2)	O5–C6–N2	126.9 (7)
O6[a]–Mn–O8	85.1 (2)	O5–C6–C7	117.2 (6)
O6[a]–Mn–O9	89.0 (2)	N2–C6–C7	115.8 (6)
O8–Mn–O9	173.0 (2)	O4–C7–O6	124.5 (7)
Mn–O1–C2	112.1 (5)	O4–C7–C6	115.7 (6)
Mn–O2–C1	111.8 (5)	O6–C7–C6	119.8 (6)

[a] Symmetry operations: (a) $1 - x, y - {}^1/_2, {}^1/_2 - z$; (b) $1 - x, y + {}^1/_2, {}^1/_2 - z$.

Magnetic Measurements. In the 3–300 K temperature range, these were carried out with a Faraday-type magnetometer equipped with a helium continuous-flow cryostat. $HgCo(NCS)_4$ was used as a susceptibility standard. Diamagnetic correction for **2** was taken as -140×10^{-6} cm^3 mol^{-1}. Magnetic anisotropy measurements for **1** and magnetization measurements for **2** in the 0–300-G field range were carried out with a laboratory-made low-field SQUID magnetometer.[36] Magnetization data above 400 G were recorded with a laboratory-made apparatus working according to the extraction method.

Description of the Structure of 2. Comparison with 1

2 forms ordered bimetallic chains running along the b-axis direction. One such chain is shown in Figure 1, projected approximately down the c axis. Bond lengths and angles involving non-hydrogen atoms are given in Tables III and IV. The Mn atom has slightly elongated octahedral surroundings; the equatorial

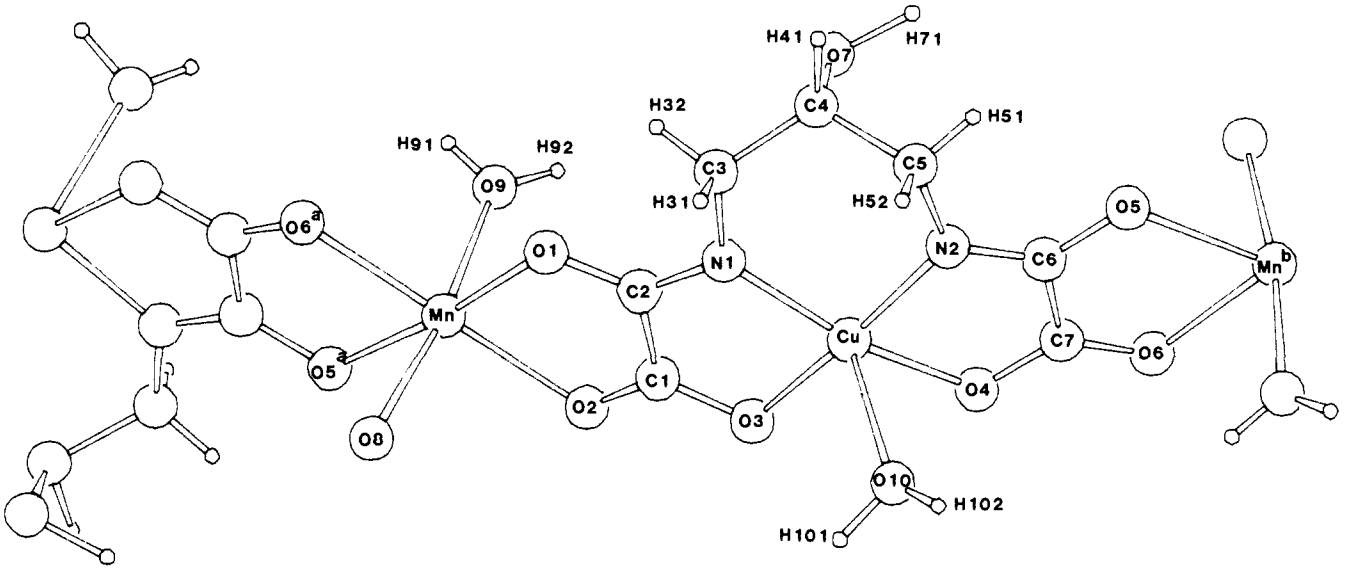

Figure 1. Section of the bimetallic chain in $MnCu(pbaOH)(H_2O)_3$ (**2**) as viewed approximately down the crystallographic *c* axis. The atomic numbering scheme used is shown.

Table V. Hydrogen Bonds in $MnCu(pbaOH)(H_2O)_3$ (**2**)

D	A	D···A, Å	∠D–H···A, deg
O7 (*x*, *y*, *z*)	O10 ($-^1/_2 + x$, $^1/_2 - y$, $-z$)	3.016 (7)	151 (1)
O8 (*x*, *y*, *z*)	O3 ($^1/_2 - x$, $-y$, $^1/_2 + z$)	2.736 (7)	
O8 (*x*, *y*, *z*)	O5 ($1 - x$, $-^1/_2 + y$, $^1/_2 - z$)	2.745 (8)	
O9 (*x*, *y*, *z*)	O1 (*x*, *y*, $z - 1$)	2.712 (8)	123 (1)
O9 (*x*, *y*, *z*)	O7 ($^1/_2 - x$, $-y$, $-^1/_2 + z$)	2.825 (8)	172 (1)
O10 (*x*, *y*, *z*)	O4 (*x*, *y*, $z + 1$)	2.779 (8)	104 (1)
O10 (*x*, *y*, *z*)	O5 ($^1/_2 + x$, $^1/_2 - y$, $-z$)	3.001 (7)	136 (1)

positions are occupied by oxygen atoms from the oxamato bridges and the apical positions by water molecules. The Cu atom has approximately square-pyramidal surroundings; two nitrogen and two oxygen atoms from the pbaOH ligand are in the basal plane while a water molecule occupies the apical position with a Cu–O10 bond length of 2.417 (6) Å. The Cu atom is displaced by 0.24 Å from the basal plane toward the apical water molecule. Each bridging group O1, O2, O3, N1, C1, C2 and O4, O5, O6, N2, C6, C7 is almost planar; the dihedral angle between the two planes is 156.5°. The chains are linked together through hydrogen bonding. A list of hydrogen bonds is given in Table V.

The separations between neighboring metal ions within the chain are Mn···Cu = 5.379 (1) Å and Cu···Mn^b ($1 - x$, $y + ^1/_2$, $^1/_2 - z$) = 5.433 (1) Å. The shortest metal···metal separations occur between metal atoms belonging to chains related by a unit-cell translation along the *c* axis: Cu···Cu^c = Mn···Mn^c = 5.073 (10) Å. The Cu···Mn^c separations involving chains related by a +1 and −1 unit-cell translation along *c* are equal to 6.482 and 7.908 Å, respectively. Between chains half a unit cell apart in the *a* direction, the closest metal···metal separations are the following: Cu···Mn^d ($^3/_2 - x$, $-y$, $^1/_2 + z$) = 5.751 (1) Å, Cu···Mn^e ($^3/_2 - x$, $-y$, $-^1/_2 + z$) = 6.398 (1) Å, Mn···Mn^d = 6.921 (1) Å, and Cu···Cu^f ($^1/_2 + x$, $^1/_2 - y$, $1 - z$) = 7.120 (1) Å.

The first difference to notice between the crystal structures of **1**[22] and **2** concerns the space groups: *Pnma* for **1** and $P2_12_12_1$ for **2**. In **1**, the Mn atoms are located on a symmetry center and the Cu atom is located in a mirror plane, whereas in **2** these symmetry requirements have disappeared. Despite the relaxation of crystallographic symmetry restrictions in **2**, the individual chains are very similar in the two compounds. The slight zigzag feature of the chain is however somewhat more pronounced in **2**. This is reflected in the slightly shorter *b* lattice parameter in **2** although the average Cu···Mn separation within the chain (5.406 Å) conforms very well with the corresponding distance in **1** (5.412 Å).

The cell dimensions of **2** are smaller than those of **1**. The main reason for this is that **2** crystallizes without the water molecule of crystallization. This brings the chains closer to one another. The shortest metal···metal separations between neighboring chains in the *a* direction are Cu···Cu = 6.545 Å and Mn···Mn = 6.977 Å in **1** and Cu···Mn = 5.751 Å and 6.398 Å in **2**. Such a difference between **1** and **2** concerning the relative positions of the chains along the *a* direction may be described as follows: in **2**, as compared to **1**, every other chain is displaced by slightly less than half of a repeat unit along *b*, as schematized by

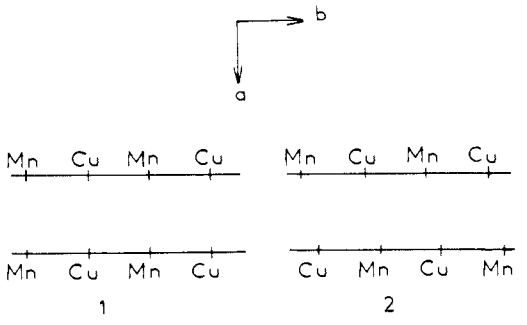

In both compounds, the chains closest to one another are those related by a unit-cell translation along *c*. In **1**, we have Cu···Cu^c = Mn···Mn^c = 5.2105 Å, and in **2**, Cu···Cu^c = Mn···Mn^c = 5.073 Å. The crystal packings for **1** and **2** are compared in Figure 2.

Magnetic Susceptibilities

We consider successively the two temperature ranges above (HT range) and below (LT range) 30 K.

30 < *T* < 300 K. In this HT range, compounds **1** and **2** have exactly the same magnetic behavior within the experimental uncertainties. This behavior is typical of antiferromagnetically coupled $Mn^{II}Cu^{II}$ chains.[19-26] At 300 K, $\chi_M T$, χ_M being the molar magnetic susceptibility per MnCu unit, is close to what is expected for isolated Mn^{II} and Cu^{II} ions with $S_{Mn} = ^5/_2$ and $S_{Cu} = ^1/_2$ local spins, respectively. Upon cooling, the first state to be thermally depopulated is that of highest spin multiplicity, where all the spins are aligned along a same direction. It follows that $\chi_M T$ smoothly decreases. At 115 K, $\chi_M T$ reaches a minimum and then increases rapidly. This minimum of the $\chi_M T$ versus *T* plot is due to the fact that, in spite of the antiferromagnetic nature of the intrachain

(23) Pei, Y; Kahn, O.; Sletten, J. *J. Am. Chem. Soc.* **1986**, *108*, 3143.
(24) Drillon, M.; Coronado, E.; Beltran, D.; Curely, J.; Georges, R.; Nugteren, P. R.; de Jongh, L. J.; Genicon, J. L. *J. Magn. Magn. Mater.* **1986**, *54–57*, 1507.
(25) Verdaguer, M.; Julve, M.; Michalowicz, A.; Kahn, O. *Inorg. Chem.* **1983**, *22*, 2624.
(26) Verdaguer, M.; Gleizes, A.; Renard, J. P.; Seiden, J. *Phys. Rev. B: Condens. Matter* **1984**, *29*, 5144.

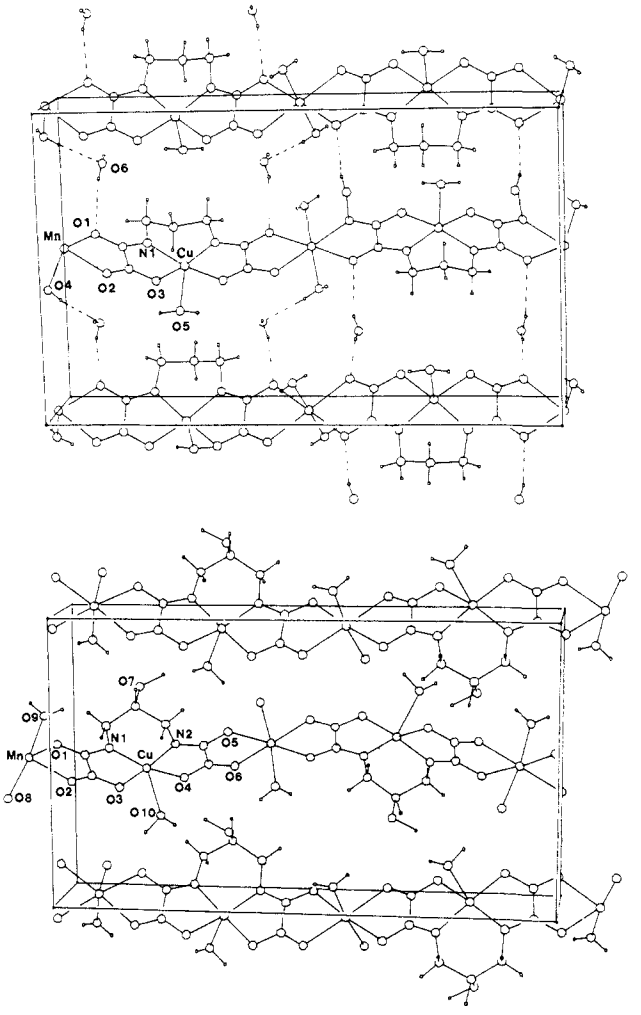

Figure 2. Perspective view of three neighboring chains in MnCu(pba)$(H_2O)_3 \cdot 2H_2O$ (**1**) (top) and in MnCu(pbaOH)$(H_2O)_3$ (**2**) (bottom). The origin of the unit cell is in the upper left-hand corner; the *a* axis runs top to bottom of page and the *b* axis left to right.

interaction between nearest-neighbor Mn^{II} and Cu^{II} ions, the chain $(MnCu)_N$ qualitatively behaves like a chain of $N/2$ ferromagnetically coupled $S = S_{Mn} - S_{Cu} = 2$ local spins for $T < 115$ K. Consequently $\chi_M T$ presents a divergence for T approaching zero and N becoming infinitely large. A quantitative model to interpret the magnetic behavior of such a $Mn^{II}Cu^{II}$ chain has been proposed. It consists of taking S_{Mn} as a semiquantum spin and S_{Cu} as a pure quantum spin.[26] The appropriate spin Hamiltonian in presence of the applied field H is eq 1, with $S_{2i-1} = S_{Mn}$, $S_{2i} = S_{Cu}$, and

$$\mathcal{H} = -J\sum_{i=1}^{N} S_{2i}\cdot(S_{2i-1} + S_{2i+1}) + g\beta H\cdot(S_{2i-1} + S_{2i}) \quad (1)$$

$S_{2N+i} = S_i$. In (1), the local g_{Mn} and g_{Cu} factors are assumed to be isotropic and equal ($g_{Mn} = g_{Cu} = g$). This model leads to numerical results that can be reasonably well fitted by the empirical expression[19] given in eq 2, with $X = |J|/kT$. (2) is valid

$$\chi_M T = (g^2/4)(4.75 - 1.62370X + 2.05042X^2 - 4.52588X^3 - 8.64256X^4)/(1 + 0.77968X - 1.56527X^2 - 1.57333X^3 - 0.11666X^{4.5}) \quad (2)$$

for $J < 0$ and $X < 0.752$. The least-squares fitting of the experimental data for **1** and **2** leads to $J = -23.4$ (4) cm^{-1} and $g = 1.97$ (2). The $\chi_M T$ versus T plot for **1** has already been represented, and that for **2** is given in Figure 3.

$T < 30$ K. In this LT range, $\chi_M T$ increases upon cooling from 30 K for both **1** and **2**; however, this increase is more rapid for **2** than for **1**. The lower the temperature is, the more pronounced this difference. For instance, at 20 K, $\chi_M T = 7.3$ cm^3 mol^{-1} K for **1** and 8.4 cm^3 mol^{-1} K for **2**, and at 10 K, $\chi_M T = 11.4$ cm^3 mol^{-1} K for **1** and 16.7 cm^3 mol^{-1} K for **2**. In the very low temperature range, below 5 K, the two compounds behave quite differently. **1** exhibits a maximum of $\chi_M T$ at 2.3 K and a maximum of χ_M at 2.2 K, due to the onset of a 3D antiferromagnetic ordering.[22] In contrast, $\chi_M T$ for **2** diverges in the low-temperature range. Below 4.6 K, the magnetic susceptibility of **2** becomes strongly field dependent, which suggests that a ferromagnetic transition takes place. We shall see below that the magnetization measurements confirm that a 3D ferromagnetic ordering actually occurs.

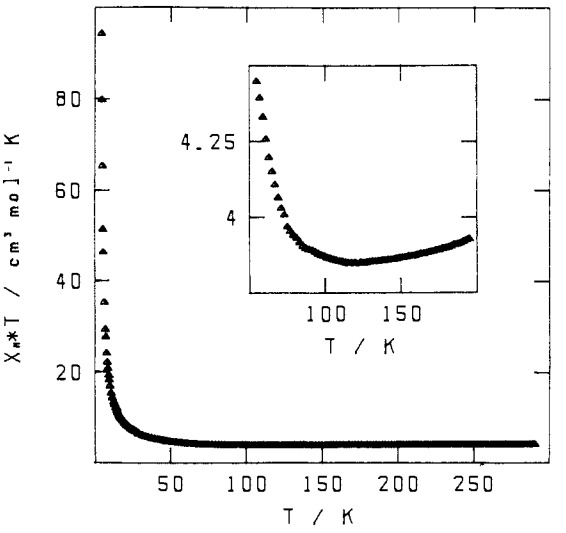

Figure 3. Temperature dependence of $\chi_M T$ for MnCu(pbaOH)$(H_2O)_3$ (**2**).

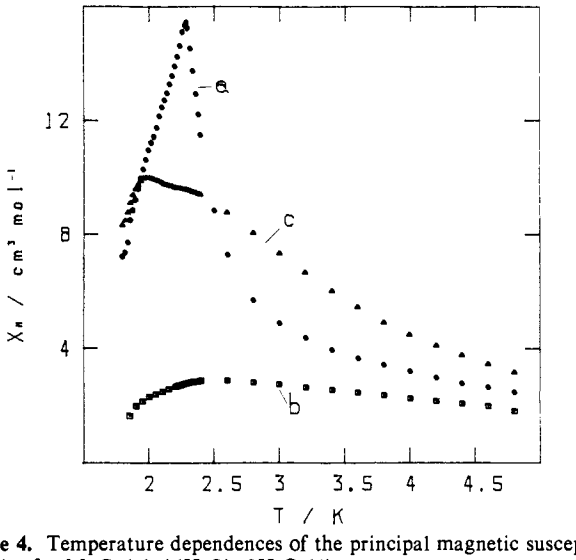

Figure 4. Temperature dependences of the principal magnetic susceptibilities for MnCu(pba)$(H_2O)_3 \cdot 2H_2O$ (**1**).

To get new insight on the magnetic structure of **1** that orders antiferromagnetically around 2.2 K, we measured the principal magnetic susceptibilities χ_a, χ_b, and χ_c along the three directions of the orthorhombic lattice in the 1.8–5 K temperature range. The results are shown in Figure 4. Down to 2.6 K, we have $\chi_c > \chi_a > \chi_b$. Consequently, the chain axis *b* is the hard axis, the *a* axis the intermediate axis, and the *c* axis the easy axis. Thus, the local spins of the ferrimagnetic chains are preferably aligned along the *c* axis. In the 1.9–2.3 K temperature range, χ_b and χ_c present a maximum corresponding to the 3D antiferromagnetic ordering of the ferrimagnetic chains. In the antiferromagnetic phase, the spin structure may be schematized as shown in Figure 5. One can notice that the 3D ordering in **1** is likely a complicated process. Indeed, χ_c actually presents two maxima at 2.3 and 1.95 K, respectively. Moreover, below 2.5 K, χ_a becomes larger than χ_c and presents a very sharp maximum at 2.3 K. Such behavior of

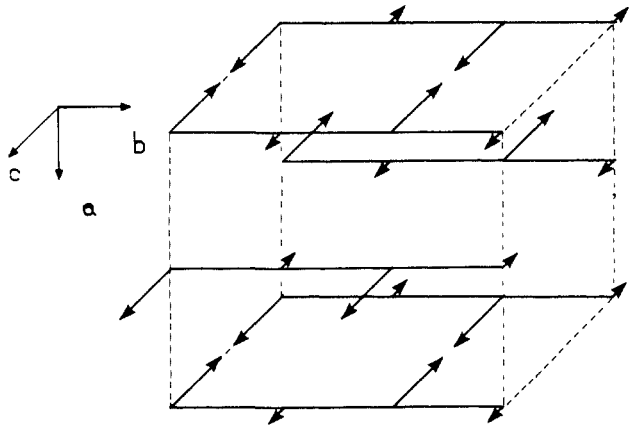

Figure 5. Schematic representation of the magnetic structure of **1** in the antiferromagnetic phase. The small canting along the *a* axis has not been represented.

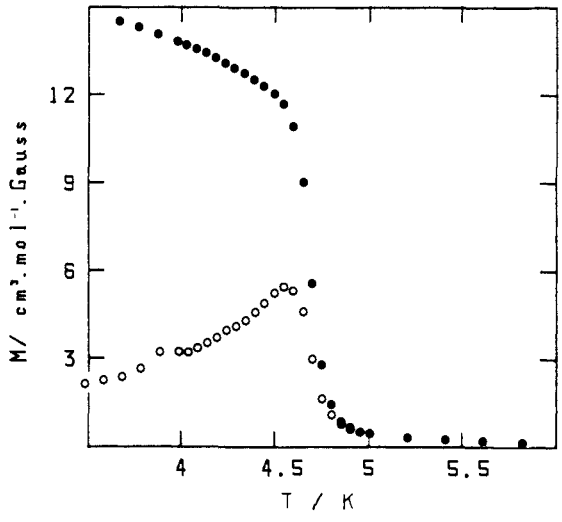

Figure 6. Temperature dependence of the magnetization M for MnCu(pbaOH)$(H_2O)_3$ (**2**) in the 6–3.5 K temperature range and a field of 3 × 10^{-2}G: ●, FCM; ○, ZFCM. See text.

χ_a most likely reveals a weak canting of the spins in the *a* direction, with a nonzero resulting moment along this direction. Such a weak ferromagnetism has already been reported for copper(II) chain compounds with intrachain ferromagnetic and interchain antiferromagnetic interactions.[15,27,28]

Magnetization Studies for 2

To confirm the ferromagnetic transition in **2**, we first studied the variation of the molar magnetization M versus T in fields between 3 × 10^{-2} and 10 G on a powder sample, with a SQUID magnetometer. The field-cooled magnetization (FCM) and zero-field-cooled magnetization (ZFCM) curves at 3 × 10^{-2} G are represented in Figure 6. The former curve (FCM) obtained on cooling down in the field shows the typical features of a ferromagnetic transition, i.e. a rapid increase of M when T decreases below 5 K and a break in the curve around T_c = 4.6 K. When the field is increased above 1 G, the ferromagnetic transition becomes less abrupt. The latter curve (ZFCM) is obtained by cooling down to 3.5 K in zero field and then applying the field and heating. At a given temperature below T_c, the ZFCM is smaller than the FCM, due to the fact that in this temperature range the applied field is too weak to move the domain walls. The ZFCM exhibits a maximum around T_c, as expected for a polycrystalline ferromagnet.[29] We also cooled the sample down to 3.5 K in the field and then switched off the field; we observed a remnant magnetization that vanishes at T_c.

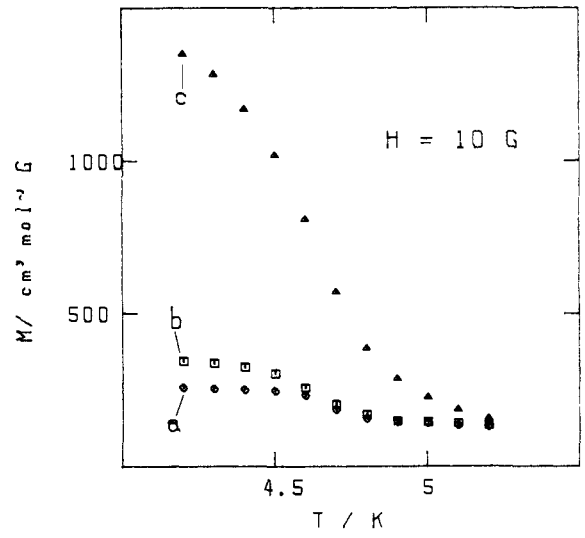

Figure 7. Temperature dependences of the principal magnetizations M_a, M_b, and M_c with H = 10 G for MnCu(pbaOH)$(H_2O)_3$ (**2**).

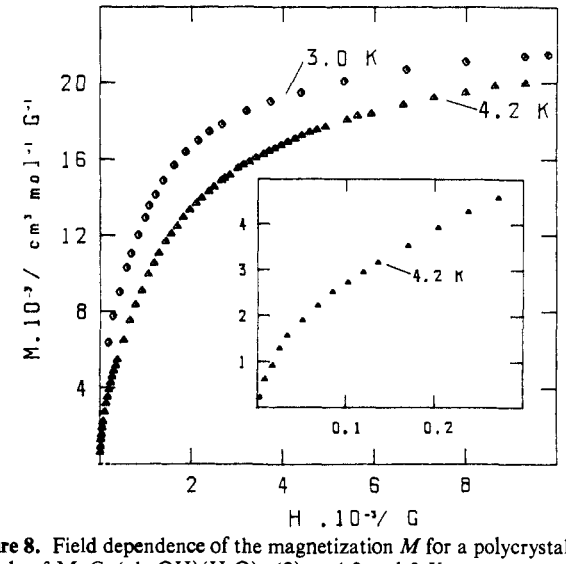

Figure 8. Field dependence of the magnetization M for a polycrystalline sample of MnCu(pbaOH)$(H_2O)_3$ (**2**) at 4.2 and 3 K.

We then studied the variation versus T of the molar magnetizations M_a, M_b, and M_c along the principal axes of the orthorhombic lattice in the 5–2 K temperature range. The results obtained with H = 10 G are shown in Figure 7. We worked with an extremely small crystal (3.7 × 10^{-6} g). Indeed, it has not yet been possible to grow larger and well-shaped single crystals. Fortunately, our SQUID magnetometer has a very high sensitivity and we were able to show that at any temperature and any field up to 20 G we have $M_c \gg M_a > M_b$. Therefore, as in **1**, the *c* axis is the easy magnetization axis. In the three directions *a*, *b*, and *c*, the difference between FCM and ZFCM at a given temperature below T_c is smaller than with a polycrystalline powder. This is due to the fact that crystal has obviously less defects than the powdered sample, so that the domain walls move more freely.

In a third step, we investigated the variation of M versus the applied field H for a polycrystalline sample. The curves at 4.2 and 3.0 K are shown in Figure 8. These curves reveal the following: (i) There is no field range, except maybe for H smaller than a few tens of Gauss, where M varies linearly versus H. (ii) The slope of the M versus H plot is extremely large in zero field and regularly decreases when H increases. The average zero-field susceptibility $(dM/dH)_{H=0}$ is equal to 75 (3) cm^3 mol^{-1} at 4.2 K and increases upon cooling. For a perfect ferromagnetic crystal, the zero-field susceptibility along the easy magnetization axis is expected to be infinite for $T \ll T_c$. In fact, a real crystal is limited

(27) Carlin, R. L. *Magnetochemistry*; Springer-Verlag: Berlin, Heidelberg, 1986.
(28) Kopinga, K.; Tinus, A. M. C.; de Jongh, W. J. M. *Phys. Rev. B: Condens. Matter* **1982**, *25*, 4685.
(29) See, for instance: Hitzfeld, M.; Ziemann, P.; Buckel, W.; Claus, H. *Phys. Rev. B: Condens. Matter* **1984**, *29*, 5023.

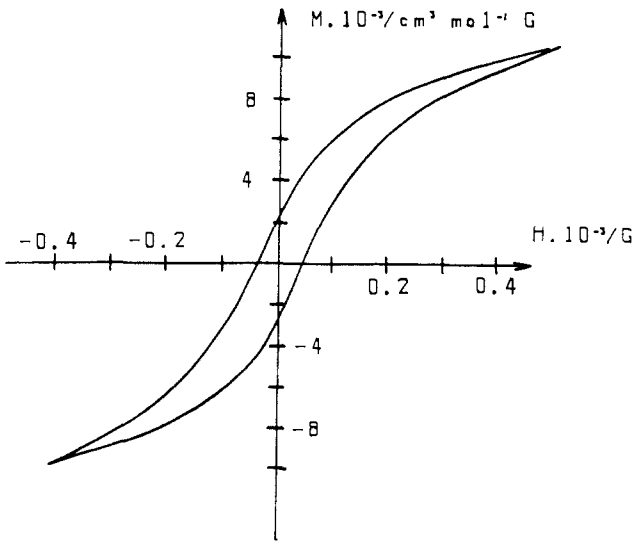

Figure 9. Hysteresis loop $M = f(H)$ for a polycrystalline sample of $MnCu(pbaOH)(H_2O)_3$ (**2**) at 1.3 K.

by a surface, which creates a demagnetization field opposite to the applied field, so that the zero-field susceptibility takes a finite value.[27] For a powder sample, the reduction of the zero-field susceptibility is even more pronounced; indeed, the susceptibility is averaged over all directions, including the hard magnetization direction. Moreover, the motions of the Bloch walls are constricted by defects and impurities. (iii) The increase of M versus H is faster and the saturation is more quickly reached at 3 than at 4.2 K. The saturation magnetization M_S may be calculated by eq 3, where

$$M_S = Ng\beta S \tag{3}$$

N is Avogadro's number and β the electronic Bohr magneton. With $S = S_{Mn} - S_{Cu} = 2$ and $g = 2$, M_S is calculated as 23.3×10^3 cm^3 mol^{-1} G. At 3 K, half of the saturation is reached at 600 G and two-thirds of the saturation at 900 G.

Finally, we investigated the magnetic hysteresis at various temperatures between 4.2 and 1.3 K. At 4.2 K the hysteresis effect is very weak. It becomes more pronounced when T decreases. The hysteresis loop at 1.3 K is shown in Figure 9. At this temperature, the remnant magnetization is equal to 2.25×10^3 cm^3 mol^{-1} G, i.e. about one-tenth of the calculated saturation magnetization, and the coercive field is about 50 G.

Discussion

In this section we discuss the possible mechanism of the three-dimensional magnetic ordering in **1** and **2**. This discussion will be based on comparison between the crystal structures of the two compounds. Indeed, it is clear that the drastic differences of the low-temperature magnetic properties arise from the small structural changes between **1** and **2**.

In both **1** and **2**, we have $Mn^{II}Cu^{II}$ ordered bimetallic chains with oxamato bridges between adjacent Mn^{II} and Cu^{II} ions. These bridges are well-known to favor an exceptionally strong antiferromagnetic interaction in spite of the relatively large separation between the metal centers, provided that there is a xy-type magnetic orbital on each metal ion.[6] The magnitude of the interaction is then due to the overlap of the magnetic orbitals on either side of the bridge, as schematized:

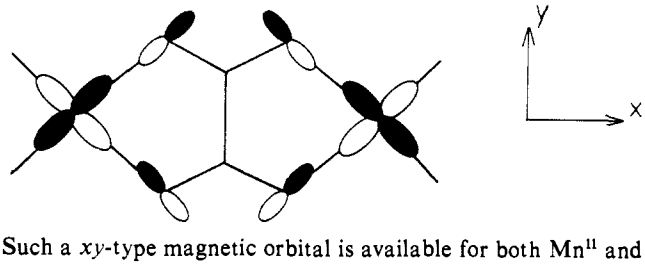

Such a xy-type magnetic orbital is available for both Mn^{II} and Cu^{II}. Since the geometry of the chains is essentially unchanged by the presence of the OH group on the central carbon atom of the propylene group in **2**, it is not surprising that in the whole temperature range where the interchain interactions play a negligible role the two compounds exhibit the same $\chi_M T$ versus T plot. For both **1** and **2**, at high temperature, $\chi_M T$ tends toward the paramagnetic limit; the minimum of $\chi_M T$ at 115 K corresponds to a short-range order state where the spins $S_{Mn} = {}^5/_2$ and $S_{Cu} = {}^1/_2$ of adjacent ions are antiparallel, but without correlation between neighboring $Mn^{II}Cu^{II}$ units. When T decreases below 115 K, the correlation length within the chain increases, leading in absence of interchain interaction, to a magnetic short-range order defined as the one-dimensional ferrimagnetism.

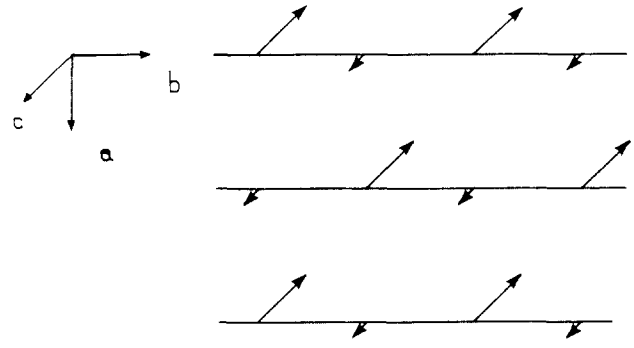

Figure 10. Schematic representation of the magnetic structure in the ab planes for **2** (see text).

The main difference between the crystal structures of **1** and **2** concerns the packing of the chains along the a direction. In **1**, the shortest interchain separations along this direction of Mn···Mn and Cu···Cu, whereas in **2** they are Mn···Cu. The Mn^{II} ion has the high-spin d^5 electronic configuration. Consequently, it most likely interacts with any other neighbor ion in an antiferromagnetic fashion.[13] Indeed, whatever the geometry of the system may be, at least one of the five magnetic orbitals centered on Mn^{II} gives a nonzero overlap with a magnetic orbital centered on the neighbor ion. If this assumption is true, the relative positions of the chains along a in **1** lead to a cancellation of the resulting spin in the ab plane, as shown in Figure 5. In contrast, the displacement of every other chain in the ab plane of **2** by roughly half of a repeat unit along b leads to a parallel alignment of the $S_{Mn} = {}^5/_2$ local spins. This situation is schematized in Figure 10, where we took into account that the easy magnetization axis is the c axis. To sum up the discussion concerning the ab planes, we can say that in the assumption where all the interactions between pairs of neighbor ions, within the chains as well as between the chains, are antiferromagnetic, these planes are antiferromagnetic in **1** and ferromagnetic in **2**.

We have to examine now how the ab planes separated by one unit cell translation along c are related. For both **1** and **2**, the shortest separations along this direction are Mn···Mn and Cu···Cu, which should favor an antiferromagnetic coupling of the ab planes. This is consistent with the 3D antiferromagnetic ordering observed in **1**, but not with the 3D ferromagnetic ordering observed in **2**. We suggest the following explanation. The interactions, intra- as well as interchain, within the ab planes are not purely isotropic but lead to an easy magnetization axis along c, i.e. perpendicular to the planes. The ferromagnetic ordering in **2** would then be due to the magnetic dipolar interactions between the ab planes. These interactions that vary as the square of the local spin momenta would be particularly important owing to the presence of $S_{Mn} = {}^5/_2$ spins. Moreover, the interchain separation along c in **2** is rather short with Mn···Mn = Cu···Cu = 5.073 Å. To check this hypothesis, we are carrying out a theoretical calculation of the magnetic dipolar interactions in both **1** and **2**. If our hypothesis is correct, compound **2** may be described in terms of ferrimagnetic chains along b with a large intrachain interaction; these chains are exchange coupled in a ferromagnetic manner in the ab planes with a preferred spin orientation along c. Owing to this anisotropy, the dipolar interactions between magnetic planes lead to the observed ferromagnetic transition. In other words, the long-range

ordering of the ferromagnetic planes *ab* would be due to the anisotropic component of the exchange.[30,31] It is likely relevant to recall here that two-dimensional ferromagnetism has been observed in A_2CrCl_4 compounds where A^+ is a bulky alkylammonium cation isolating magnetically the ferromagnetic $CrCl_4^{2-}$ layers,[32,34] as well as in similar tetrachlorocuprate compounds.[34,35]

One of the aspects of the discussion above deserves some additional comment, namely the ferromagnetism versus ferrimagnetism problem. Two nonequivalent spin sublattices NS_A and NS_B, with $S_A \neq S_B$, may interact to give either a ferromagnetic structure $N(S_A + S_B)$ or a ferrimagnetic structure $N(|S_A - S_B|)$. Thus, the only alternative to the ferrimagnetism is the ferromagnetism and not the antiferromagnetism. Consequently, it is quite appropriate to define the ground state of the $Mn^{II}Cu^{II}$ ordered chains as one-dimensional ferrimagnetism. If the Mn^{II}–Cu^{II} intrachain interaction was ferromagnetic instead of antiferromagnetic, we would speak of one-dimensional ferromagnetism. Let us consider now the interactions between the chains within the *ab* plane. We have seen that these interactions can lead either to the situation encountered in **1** with a cancellation of the spins or to that encountered in **2** with a parallel alignment of the $S_{Mn} = {}^5/_2$ spins. Since the former alternative clearly corresponds to antiferromagnetism, the latter one must be defined as ferromagnetism and it is correct to say that in **2** the ferrimagnetic chains couple ferromagnetically within the *ab* plane. Of course, if the interchain interactions in the *ab* plane became of the same order of magnitude as the intrachain interaction, the one-dimensional character of the system would vanish. In that case, it would be more appropriate to describe the situation in terms of ferrimagnetic *ab* planes.

(30) Mermin, N. D.; Wagner, H. *Phys. Rev. Lett.* **1966**, *17*, 1133.
(31) Stanley, H. E.; Kaplan, T. A. *J. Appl. Phys.* **1967**, *38*, 3.
(32) Day, P. *Acc. Chem. Res.* **1979**, *12*, 236.
(33) Bellitto, C.; Day, P.; Wood, T. E. *J. Chem. Soc., Dalton Trans.* **1986**, 847.
(34) de Jongh, L. J.; Miedema, A. R. *Adv. Phys.* **1974**, *23*, 1.
(35) Estes, W. E.; Losee, D. B.; Hatfield, W. E. *J. Chem. Phys.* **1980**, *72*, 630.
(36) Beauvillian, P.; Chappert, C.; Renard, J. P. *J. Phys. E: Sci. Instrum.* **1985**, *18*, 839.
(37) Cromer, D. T.; Waber, J. T. *International Tables for X-ray Crystallography*; Kynoch: Birmingham, 1974; Vol. IV, p 99 (Table 2.2B).
(38) Frenz, B. A. *The SDP-User's Guide*; Enraf-Nonius: Delft, The Netherlands, 1983.

Conclusion

In this paper, we have described an original strategy to design molecular-based systems ordering ferromagnetically. The basis idea is to assemble ferrimagnetic chains within the crystal lattice in a ferromagnetic fashion. Our approach has been the following: (i) The interaction within the chains should be as large as possible and the local spins of the adjacent ions as different as possible; these conditions led us to the choice of the systems $Mn^{II}Cu^{II}$ with oxamato-type bridges. (ii) The shortest interchain metal–metal separations should be of the type Mn···Cu rather than Mn···Mn and Cu···Cu. By making some subtle chemical modifications, we have succeeded in synthesizing compound **2** with such relative positions of the chains along one of the directions of the lattice. This compound has actually been found to order ferromagnetically at $T_c = 4.6$ K. Below T_c, it exhibits a hysteresis loop rather typical of a soft magnet. The easy magnetization axis has been determined; it is the *c* axis. Unfortunately, due to the small size of the single crystals, we have not been able to plot the magnetization versus field curve along this axis. We have only investigated the magnetization of a polycrystalline sample. The magnetization is then restrained by the anisotropy field.

The area of the molecular ferromagnets is in its infancy. Several groups over the world work along this perspective by using various strategies. This emulation should favor a fast development. The main goals are first to shift T_c toward higher temperatures but also to design stable systems, given a well-defined hysteresis loop with large remnant magnetization and coercive field. We think that our approach utilizing both the efficiency of the organic based ligands to transmit the electronic effects on long distances and the specific ability of the d-metal orbitals to provide high magnetic moments will allow us to report on novel systems of this kind in the near future.

Acknowledgment. We thank Professor L. J. de Jongh for very stimulating discussions.

Registry No. 1, 101935-07-3; **2**, 105121-18-4; **3**, 99387-35-6; **4**, 105139-32-0; 2-hydroxy-1,3-propylenediamine, 616-29-5; ethyl oxamate, 617-36-7.

Supplementary Material Available: Tables VI and VII giving anisotropic thermal parameters for Mn and Cu atoms and positional parameters for hydrogen atoms (2 pages). Ordering information is given on any current masthead page.

The Generation, Microwave Spectrum, and Structure of Propadienethione, $H_2C{=}C{=}C{=}S$

R. D. Brown,* K. G. Dyall, P. S. Elmes, P. D. Godfrey, and D. McNaughton

Contribution from the Department of Chemistry, Monash University, Clayton, Victoria, Australia 3168. *Received August 24, 1987*

Abstract: The third member of the cumulene-thione series H_2C_nS, propadienethione, has been produced by pyrolysis of cyclopenteno-1,2,3-thiadiazole and detected by microwave spectroscopy. The rotational constants from a number of isotopomers have been used to derive a molecular geometry, which shows that propadienethione is a planar molecule of C_{2v} symmetry, unlike propadienone which is kinked. A fully optimized geometry from a set of ab initio calculations done at the MP3/6-31G** level is in agreement with the experimental results. The dipole moment has been calculated from the Stark effect to be 2.064 Debye.

The cumulenone series of molecules is of special interest, because in contradiction to the previously accepted theory of cumulated double bonds, the third member of the series, propadienone, has been shown to be kinked at the central carbon.[1-3] An analysis of the vibrational satellite spectra of H_2 and D_2 butatrienone, the fourth member of the series, has recently shown that the molecule is not kinked in its equilibrium configuration.[4]

(1) Brown, R. D.; Godfrey, P. D.; Champion, R.; McNaughton, D. *J. Am. Chem. Soc.* **1981**, *103*, 5711-5715; **1982**, *104*, 6167.
(2) Brown, R. D.; Champion, R.; Elmes, P. S.; Godfrey, P. D. *J. Am. Chem. Soc.* **1985**, *107*, 4109-4112.
(3) Brown, R. D.; Godfrey, P. D.; Champion, R. *J. Mol. Spectrosc.* **1987**, in press.

0002-7863/88/1510-0789$01.50/0